Apparent slip in colloidal suspensions

Aref Abbasi Moud, Jourdain Piette, Marziyeh Danesh, et al.

Citation: Journal of Rheology **66**, 79 (2022); doi: 10.1122/8.0000302
View online: https://doi.org/10.1122/8.0000302
View Table of Contents: https://sor.scitation.org/toc/jor/66/1
Published by the The Society of Rheology

Apparent slip in colloidal suspensions

Aref Abbasi Moud,[1] Jourdain Piette,[1] Marziyeh Danesh,[1] Georgios C. Georgiou,[2,a)] and Savvas G. Hatzikiriakos[1,a)]

[1]*Department of Chemical and Biological Engineering, The University of British Columbia, Vancouver, British Columbia V6T 1Z3, Canada*
[2]*Department of Mathematics and Statistics, University of Cyprus, P.O. Box 20537, 1678 Nicosia, Cyprus*

(Received 25 May 2021; final revision received 5 September 2021; published 29 November 2021)

Abstract

In this study, we have carried out experiments to characterize the wall slip of colloidal suspensions of kaolinites. To demonstrate slip, the rheological measurements were carried out with parallel-plate geometry with smooth and rough plates. The asperities of the rough surface penetrated the slip layer and created a nearly no-slip region, whereas the smooth plate showed significantly higher slip, a conclusion drawn by comparing the macroscopic flow curves in both cases. Two slip regimes were identified, namely, (i) an elastic slip regime below the yield stress of the suspension where the material slips like a solid and (ii) a slip regime above the yield stress where the material yields and flows. The slip velocity was quantified using a simple phenomenological slip model that seems to capture slip in both flow regimes. The transition from the first slip regime to the other has been resolved numerically as the material starts yielding first at the edge of the parallel-plate geometry with the yield point propagating inwards as the rotational speed is increased. The numerical method also establishes uniquely the yield stress value, which was found to agree with data obtained from parallel-plate, cone-and-plate, and concentric cylinder geometries.
 https://doi.org/10.1122/8.0000302

I. INTRODUCTION

Complex materials such as colloidal suspensions, microgels, emulsions, and others tend to slip at smooth surfaces [1–3]. Slip in these systems is the rule and not the exception and, therefore, such effects should carefully be considered [1]. The type of slip in these systems is only apparent as it is due to the formation of a liquid layer (depletion layer) close to the wall with particle concentration less than that in the bulk that causes a region with high velocity gradient interpreted as "apparent" slip [2–10]. The thickness of this layer has been found to be a function of particle size and concentration of suspension and there is qualitative evidence reported in the literature [2,3].

Several studies have reported on the apparent slip of complex fluids such as gels, microgels (concentrated suspensions of deformable particles), and colloidal gels/glasses [11–21]. In particular, slip has been reported for the cases of a hydroxypropyl guar gel [16], microgels of deformable particles [17–20], skin/hair care gels [20], viscoplastic hydrogels [21], and gels of colloidal particles [12,13,15]. In all these systems, the formation of a depletion layer causes apparent slip. Moreover, these diverse systems exhibit generic signatures irrespective of the composition of the dispersions and the nature of the particles (similar to the systems examined in the present work) [2]. The presence of the apparent slip complicates the rheological analysis, e.g., the determination of the true yield stress of the materials, which apparently seem to depend on the gap size of the geometry used.

The importance of slip was recognized in early studies by Mooney [22] who reported that the flow curves of materials in capillary flow under slip exhibit a dependence on the capillary radius and proposed a method to analyze slip, which is known as the Mooney technique. This is widely employed to calculate the slip velocity in other geometries as well [23]. For example, Yoshimura and Prud'homme [24] have studied the slip of clay suspensions to derive and develop a methodology to study slip using a technique similar to Mooney for flow between parallel disks (torsional flow) and rotating cylinders (Couette flow). Slip has been inferred via a variety of techniques by several reports in the literature and excellent reviews on the subject have been published [25,26].

To prevent slip, rough surfaces have been used (sandblasted and/or sandpaper of various grit sizes) in the rheological characterization of many fluids. For instance, Aral and Kalyon [27] performed a systematic study on the effects of temperature and surface roughness on wall slip of a concentrated suspension. They investigated the role played by surface roughness and observed that an increase in surface roughness prevents slip in the flow of concentrated suspensions. While sandpaper can prevent slip, the possibility of overestimating the yield stress by changing the geometry using roughness of various degrees should carefully be considered.

In this paper, we are assessing the slip effects in kaolinite suspensions at various concentrations [28]. Evidence in the literature of slip in colloidal gels is widespread. The behavior of colloidal gels possesses similar features as discussed above [29]. A generic feature of colloidal gels is the difficulty associated with suppressing slip effects even when a

[a)]Authors to whom correspondence should be addressed; electronic mail: georgios@ucy.ac.cy and savvas.hatzi@ubc.ca

rough surface is employed. It appears that specific roughness comparable to larger aggregates in the gel is vital to prevent slip. Buscall *et al.* [29] suggested a method of analyzing the rheological response of colloidal gels with and without slip and a surface yielding phenomenon correlated to the restructuring of the cluster with time. In their report, a dynamic phase diagram correlating slip to the interaction between particle and volume fraction was suggested.

A recent study concerning the case of colloidal gels formed through depletion interactions suggests that slip occurs even if the surface roughness is akin to particle's individual sizes [13]. This phenomenon was attributed to the structural changes of the gels that cause the number of bonds between the bulk of the material and the surface to diminish as the cluster size is increased. It was reported that in order to eliminate slip effects, surface roughness must be much larger than the particle sizes, probably comparable to the sizes of largest structural inhomogeneities. In this case, the effective shear geometry might change overestimating the rheological parameters.

Overall, the rheological characterization of concentrated suspensions (both in glassy and gel states) is complicated due to microstructural changes during shear flow. In general, the glassy state corresponds to high-volume particle fractions with no network present, while the gel state corresponds to low volume fractions and it is characterized by the presence of a network [30]. In the literature, shear induced migration has been proven to lead to the depletion of the particles away from moving rheometer's plates. Leighthon and Acrivos [6] suggested that shear induced migration depends on the shear rate. Ovarlez *et al.* [31] also argued that migration can be assumed to be a quasi-instantaneous observation, so its avoidance in a short span of time is impossible; however, most experiments on shear induced migration reported in the literature [32–34] indicate slow migration of particles up until volume fractions of 55%. Although migration of the particles cannot be avoided, choosing a larger gap, lower shear rate, and adjustment of concentration range may help.

In this paper, we make use of flows approximating simple shear (torsional flow between two parallel plates) to study the slip of colloidal suspensions of kaolinite particles. The methodology and the proposed model can be applied to many other colloidal systems that possess similar generic features. In fact, the behavior observed is generic particularly for suspensions exhibiting yield stress behavior [13,14,18,19]. As discussed above, the presence of yield stress complicates the rheological analysis behavior as the (apparent) yield stress depends on the characteristic dimensions of flow (distance between the parallel plates, gap between the rotational cylinders, and capillary radius). The main objective of this paper is to identify the various slip regimes present in these systems [12]. Another objective is to develop a methodology to recover through slip analysis the true rheological parameters of the materials particularly the true yield stress of the material, a contribution of the present work. These cannot always be recovered with the sole use of rough (sandpaper)/sand-blasted surfaces as discussed in the present work. Therefore, a basic and important question is whether the true yield stress of the material can be calculated through analysis of experimental results. Finally, we analyze the calculated slip with a generic phenomenological slip model that seems to capture their generic behavior resulting in the true rheological parameters of the material. More elaborate theoretical models on microgels that apply to other dispersed systems can be found elsewhere [13].

II. MATERIALS AND EXPERIMENTAL METHODS

A. Materials

The system studied is a kaolinite suspension (purchased from Sigma Aldrich with a linear formula of $Al_2O_3 \cdot 2SiO_2 \cdot 2H_2O$ and molecular weight of 258.16 g/mole). The suspensions were prepared by mixing the hydrated aluminum silicate (kaolin) powders in de-ionized water using a bench mixer for 30 min. Samples with 18.7, 25, and 31 wt. % kaolin were prepared using 30 min mechanical stirring and 60 min sonication using a sonication amplitude of 100% in the water bath to reduce the elevation of temperature and evaporation of water, thereby supplying ~2500 J/g sonication energy to the kaolinite suspensions. The kaolinite suspensions had a pH of ~6.8 and were generally stable with no significant sedimentation over a period of 24 h [35]. The exact geometrical details of the kaolinite particles used in this study are reported in [28]; these were determined by atomic force microscopy with a reported average length of ~66 nm, a diameter of 3 nm (a mean aspect ratio of 22), and a root mean squared asperity of 41 nm.

B. Experimental methods

The rheological properties were studied by using a rotational rheometer (MCR 502 Anton Paar) equipped with parallel-plate geometry (a diameter of 50 mm). The use of the large-diameter parallel-plate geometry is necessary to avoid edge effects at high shear rates [36]. The results from the parallel-plate geometry agreed well with those (additionally performed) from cone-and-plate (a diameter of 25 mm) as well as concentric cylinder (Couette flow) demonstrating minimal edge effects [36]. To avoid sample evaporation, a thin film of mineral oil was applied on the periphery of samples. All measurements were performed at the temperature of 25 °C. As these systems are susceptible to apparent slip, we have used several different gaps (0.2, 0.3, 0.5, and 1 mm) or/and sandpaper (grit size of 400 that corresponds to an average asperity size of 18.3 μm) to suppress slip effects. Steady-shear experiments were performed over the shear rate range from 0.01 to 1000 s^{-1} to capture the different slip regimes.

In order to verify the yield stress values obtained through steady-shear experiments, creep experiments were also performed using the parallel-plate geometry at the gap size of 0.7 mm.

III. RESULTS AND DISCUSSION

A. Experimental observations

1. Kaolinite suspension

Kaolinite suspensions possessing a platelet, hexagonal morphology exhibit slip behavior as shown in Fig. 1. The

flow curves of three suspensions of different concentrations (18.7, 25, and 31 wt. %) are gap dependent consistent with the assumption of slip. This behavior has been seen previously in the literature. Meeker *et al.* [18] and Seth *et al.* [19] have studied the behavior of microgels and observed similar slip behavior. Essentially, we can identify three flow regimes: (i) at stresses below an apparent "slip" yield stress, $\tau_{y,s}$ (pseudoyield stress referred to in [18,19]), the material does not flow or slip (regime I). This regime can only be reached with creep tests by applying stresses less than $\tau_{y,s}$ (ii) at higher stresses above $\tau_{y,s}$, the interface layer fails (failure of a layer in the bulk seems improbable) and the material slips (solidlike) similar to the slip of elastomers/solids (elastic regime) in simple shear flows (regime II). The "slip" yield stress is assumed to be independent of the gap, which seems to be the case in most experimental results depicted in Fig. 1 and (iii) at higher shear stress above its true yield stress, τ_y, the material moves partly due to slip and partly due to the rate of deformation (shear rate) (viscoelastoplastic, regime III). The various flow regimes are discussed below in conjunction with the proposed slip model, which captures the slip behavior of the materials in both flow regimes.

In Fig. 1, the shear stress, τ_R, at the rim of the parallel-plate rheometer has been plotted as a function of the nominal shear rate at the rim, defined as $\dot{\gamma}_n \equiv R\Omega/h$, where R is the plate radius, Ω is the angular velocity, and h is the distance between the two parallel plates. Certain corrections have been applied to the shear stress data. First, in regime II, the material behaves purely elastically with $\tau = G_o\gamma$, where G_o is an elastic modulus defining the strength of the suspension [11]. Since a linear relationship exists between the shear stress and shear strain, the shear stress at the rim is $\tau_R = 2M/\pi R^3$, where M is the torque obtained from the rheometer. This expression can be easily proven by considering the shear stress profile in cylindrical coordinates as $\tau_{r\theta} = G_o\gamma_R r/R$, where γ_R is the strain at the rim of the parallel-plate geometry. Then, the torque can be obtained via $M = 2\pi\int_o^R r\tau_{r\theta}r\,\mathrm{d}r = \pi\tau_R R^3/2$ or $\tau_R = 2M/\pi R^3$. On the other hand, in regime III, where flow begins, the relationship becomes $\tau_R = M/2\pi R^3[3 + \mathrm{d}\ln M/\mathrm{d}\ln\dot{\gamma}_R]$, and, therefore, the appropriate correction to the data in this regime has been applied. In the transition from regime II to III, the data should be corrected accordingly, which can only be done numerically (the inner core of the material is unyielded and the outer core is yielded). This is explained below when the slip model is presented and is coupled with the Herschel–Bulkley (H–B) model. The yield stress and the other parameters of the H–B model are calculated accurately together with the slip parameters.

It also stands out that in Figs. 1(b) and 1(d), the application of sandpaper with all grit size of 180–400 is successful in suppressing slip. However, at the higher concentration [Fig. 1(e)], due to the existence of a stronger network and having higher probability of slip, at identical grit size, the application of sandpaper is less successful in suppressing wall slip. We also note that the plateau defining the apparent yield stress for the case of sandpaper is overestimating the true yield stress of the material, which also seems to be dependent on the grit size of the sandpaper. While such data are useful in demonstrating the occurrence of slip and its prevention, it should be interpreted carefully with regard to the true yield stress, τ_y, and the other rheological parameters.

2. Verification of yield stress

In this section, we perform creep tests to verify the yield stresses obtained from steady-shear tests (plateau value in Fig. 1). Figure 2 shows creep experiments of kaolinite suspension with concentrations of 18.7, 25, and 31 wt. %. Typically, during a creep experiment, there exists a viscosity bifurcation [37], i.e., the material slightly starts to flow (deformation grow large) and eventually either comes to a stop at a finite strain or continues to a rapid shear phase, depending on inherent material critical stress and level of imposed stress. To report yielding, here we chose a typical accumulated strain of ~10 as a cutoff point to differentiate between yielded and unyielded (shown as a horizontal dashed line in Fig. 2). For the 18.7 wt. % sample, yielding happens at ~1.5 Pa; however, for the 25 wt. % suspension yielding occurs at a higher shear stress, 2.2 Pa. The results of creep yield stress characterization are tabulated in Table I. These agree with the values of steady shear (average plateau values over all gaps in Fig. 1) reported earlier (listed in Table I).

The strain value of 10 has been chosen arbitrarily; however, it is safe to assume that the accumulation of strain of about 10 in under 300 s is enough to conclude if a material has yielded within a practical time scale [38]. Yielding of thixotropic viscoelastic materials is a function of time as well, as material yielding is depending on the structure that evolves with time (aging). Moreover, Figs. 2(b), 2(d), and 2(f) plot the creep strain rate as a function of time, which shows more clearly yielding as the creep shear strain either declining (unyielded) with time or tending to a steady value (yielded).

To further confirm these yield stress values and to assess the corrections applied to the parallel-plate data, the flow curves of kaolinite suspensions were also determined with cone-and-plate and concentric cylinder geometries. The advantage of using the cone-and-plate geometry is that both shear stress and shear rate are constant throughout the fluid for small enough gaps. In concentric cylinders, the shear rate field is nearly uniform for gaps much smaller than the radius of the geometry. In addition, the concentric cylinder geometry does not suffer from edge effects as opposed to the parallel-plate and cone-and-plate geometries. Figure 3 displays a comparison between the flow curves of 18, 25, and 31 wt. % samples using a parallel plate (P-P) at a gap size of 0.5 mm with cone-and-plate (C-P) at a gap size of 0.047 mm and concentric cylinder (C-C) geometry with a gap size of 0.418 mm. The superimposition of flow curves from the three different geometries (particularly in the plateau region) confirms (i) the yield stress values listed in Table I and (ii) the validity of the appropriate corrections applied to the parallel-plate data. It seems that the value of the plateau truly displays the real yield stress of these suspensions and the values using sandpaper, although useful, are overestimations.

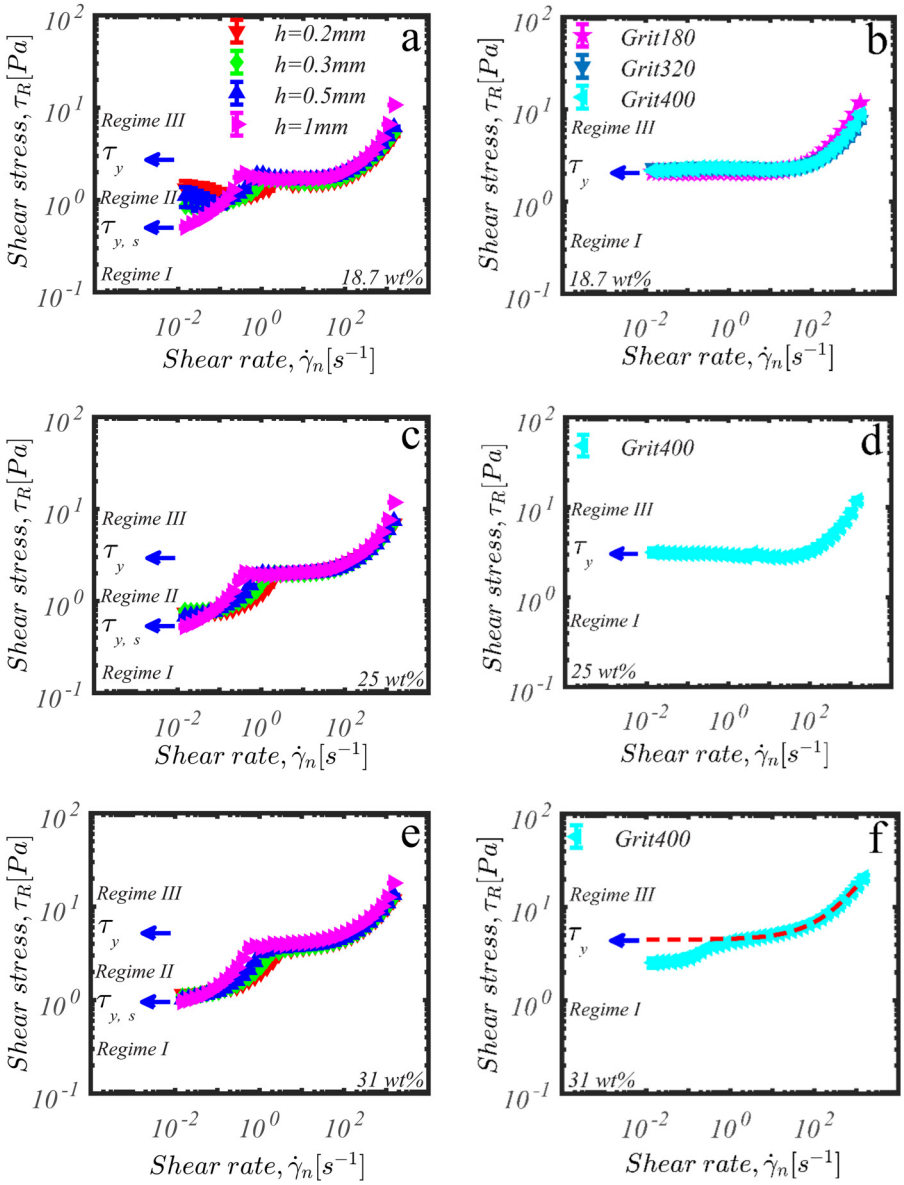

FIG. 1. (a) and (b) The effect of the gap between the parallel plates and sandpaper on the flow curves of 18.7 wt. % suspension of kaolinite without and with sandpaper, respectively, defining the various flow (slip) regimes. Regime I: the imposed stresses are too small to cause flow and/or slip; regime II: the material slips as solid (elastic flow regime) and the gap dependence of the flow curve indicate the presence of slip; and regime III: above the true yield stress where flow is partially due to slip and partially due to flow (viscoelastoplastic regime). (c) and (d) Flow curves of suspension of kaolinite with 25 wt. % concentration at gaps of 0.2–1 mm without and with sandpaper, respectively. (e) and (f) Flow curves of suspension of kaolinite with 31 wt. % concentration at gaps of 0.2–1 mm without and with sandpaper, respectively.

In fact, it appears that the use of sandpaper overestimates the yield stress (up to 25%) and flow curve of the suspensions due to alteration/uncertainty of the gap. Sandpapers of grit sizes 180–400 possess asperities in the range of 30–80 μm, which means gap uncertainty of 0.06–0.16 mm and possibly justifies the yield stress overestimation of 25%. A comment related to discrepancies between the experimental results obtained from the three different geometries in regime II seems relevant. The data in regime II show essentially the "slip" yield stress, $\tau_{y,s}$, the stress at which the interface fails for the onset of solidlike slip. The C-C involves a cylindrical interface free of edge failure, the P-P is a flat interface of a nonlinearly varying shear stress also subject to edge failure, while that of C-P is a flat interface of constant shear stress. Considering these complexities, the experimental error is expected to be significant, although overall the data depicted in Fig. 3 are consistent, except for the C-P data in Fig. 3(a).

B. The slip model

In analyzing the experimental data of Fig. 1 in regime III, the Herschel–Bulkley (H–B) equation is used, whose scalar form can be written as

$$\begin{cases} \dot{\gamma} = 0, & \tau \le \tau_y, \\ \tau = \tau_y + k\dot{\gamma}^n, & \tau > \tau_y, \end{cases} \tag{1}$$

where τ is the shear stress, $\dot{\gamma}$ is the shear rate, τ_y is the yield stress, k is the consistency index, and n is the power-law exponent.

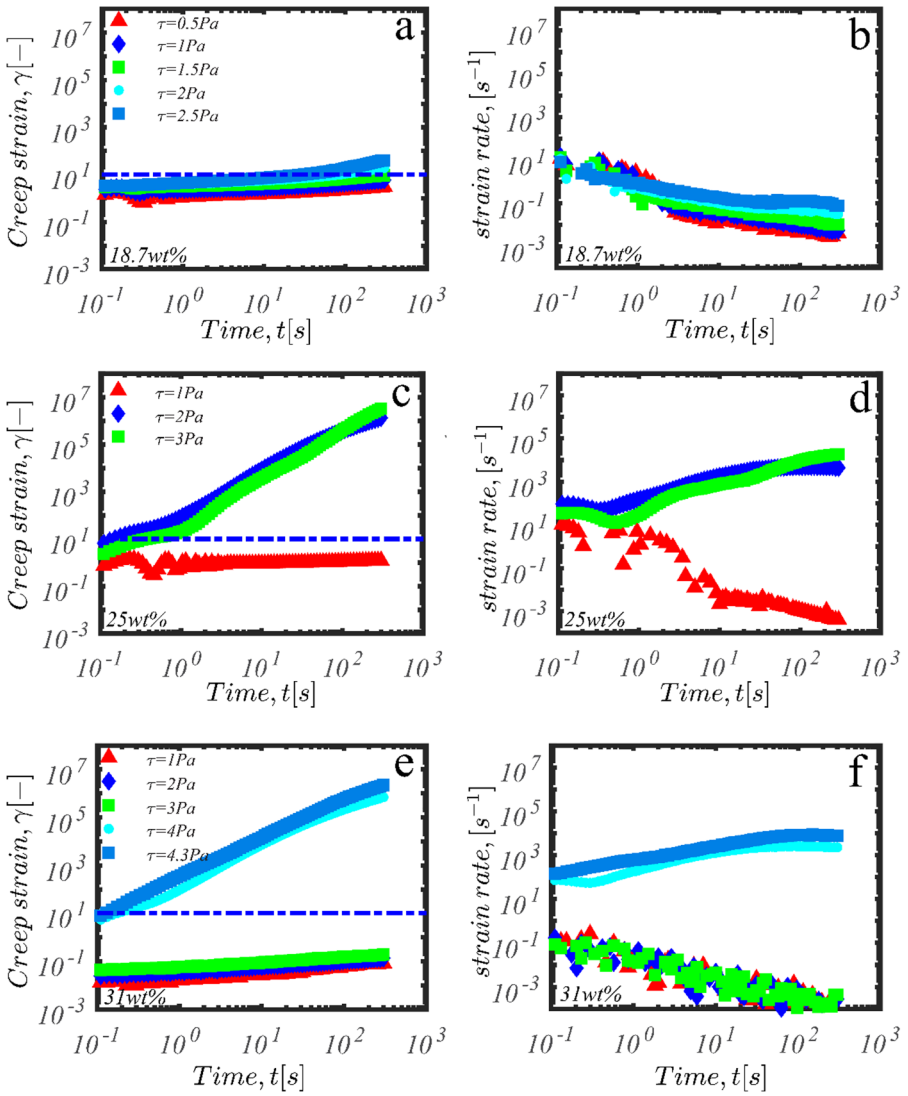

FIG. 2. Determination of yield stress via creep and creep strain rate of kaolinite suspensions with a concentration of (a) and (b) 18.7 wt. %, (c) and (d) 25 wt. %, and (e) and (f) 31 wt. %. Figures 2(b), 2(d), and 2(f) have been produced by differentiating the corresponding creep data of Figs. 2(a), 2(c), and 2(e), respectively. The creep experiments were performed with the parallel-plate geometry (50 mm in diameter, and a gap size of 0.7 mm) using rough plates with grit 400. Dashed lines represent the cutoff point of accumulated strain to yielding to define the yield stress.

Based on the above experimental observations, we hypothesize that different slip models apply in regimes II and III (discussed in the context of Fig. 1),

$$\tau_w = \tau_{y,s} + a_1 V_S^m,\ \tau_{y,s} < \tau_w \leq \tau_y \tag{2}$$

and

$$\tau_w = \bar{\tau}_{y,s} + a_2 V_S^m,\ \tau_y < \tau_w, \tag{3}$$

where τ_w is the wall shear stress, $\tau_{y,s}$ is the "slip" yield stress, V_S is the slip velocity, m is the slip exponent, and a_1 and a_2 are the slip coefficients in regimes II and III, respectively. The value of the parameter $\bar{\tau}_{y,s}$ is calculated so that when the stress is equal to the yield stress τ_y, i.e., at the transition from regime II to regime III, the two slip equations predict the same slip velocity (to avoid a discontinuity in the flow curve), that is,

$$\left.\begin{aligned}\tau_y &= \tau_{y,s} + a_1 V_S^m \\ \tau_y &= \bar{\tau}_{y,s} + a_2 V_S^m\end{aligned}\right\} \Rightarrow \frac{\tau_y - \tau_{y,s}}{a_1} = \frac{\tau_y - \bar{\tau}_{y,s}}{a_2}$$
$$\Rightarrow \bar{\tau}_{y,s} = \frac{(a_1/a_2 - 1)\tau_y + \tau_{y,s}}{a_1/a_2}. \tag{4}$$

TABLE I. Analysis of yield stress obtained via creep and steady shear experiments.

Suspension type	τ_y (Pa) Steady shear	τ_y (Pa) Creep
Kaolinite, 18.7 wt. %	1.6	1.5
Kaolinite, 25 wt. %	2.2	2
Kaolinite, 31 wt. %	3.8	4

Below, the various flow regimes are discussed in the context of Fig. 4.

Regime I: A certain nominal shear strain $\gamma_n = \Delta x/h$, where Δx is the displacement and h is the spacing between the two plates, is applied to the material, which results into a wall shear stress less than $\tau_{y,s}$. The material behaves as solid and the shear stress is related to its modulus, G_o, via

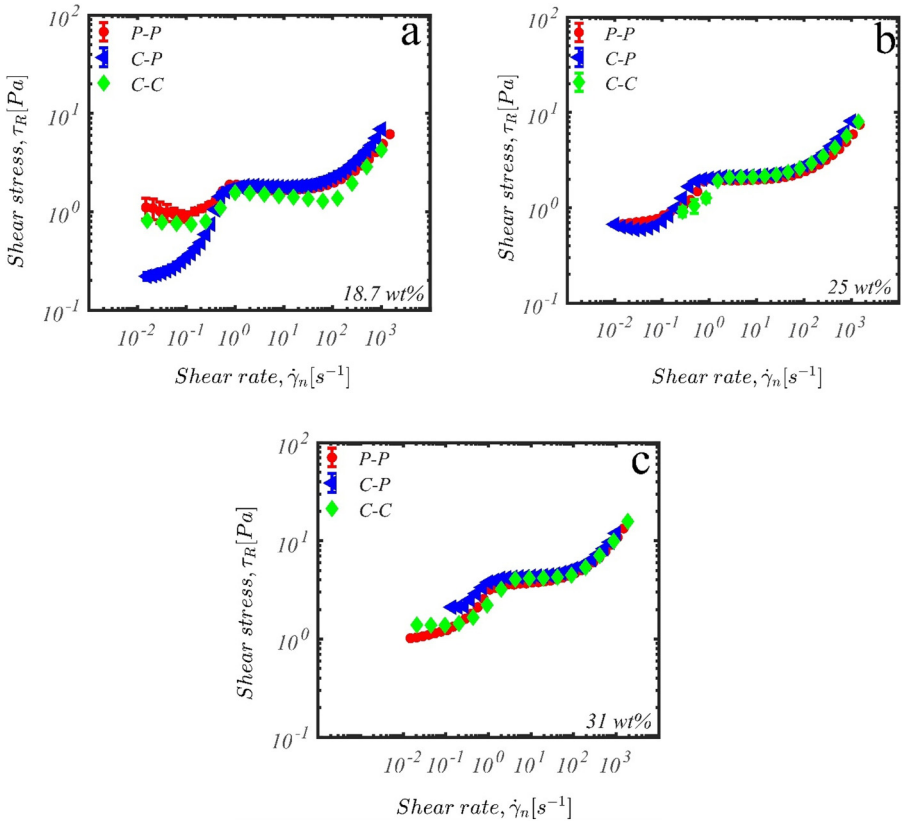

FIG. 3. (a)–(c) comparison between the flow curves of 18.7, 25, and 31 wt. % samples using a parallel plate (P-P) with a gap size of 0.5 mm, cone and plate (C-P) at a gap size of 0.047 mm and 2° angle and concentric cylinder (C-C) geometry at a gap size of 0.418 mm.

$\tau_w = G_o\gamma$. The nominal strain in this flow regime, γ_n, is equal to the true strain, γ imposed to the material. Once a critical strain, γ_C, is reached the material starts slipping in a solidlike manner. At this point, $\tau_{y,s} = G_o\gamma_C$.

Regime II: In this regime, the material still behaves like a solid as the applied stresses are below the yield stress, τ_y. However, the interface is not strong enough to withstand these shear stresses and as a result apparent slip is observed following Eq. (2). To calculate the flow curve in regime II, we use $V_S = \dot{\gamma}_n h/2$ (complete slip), where $\dot{\gamma}_n$ is the nominal shear rate defined as the velocity of the upper plate normalized by the gap spacing, h. Substituting into Eq. (2), we obtain

$$\tau_w = \tau_{y,s} + a_1(\dot{\gamma}_n h/2)^m, \quad \tau_{y,s} < \tau_w \le \tau_y. \tag{5}$$

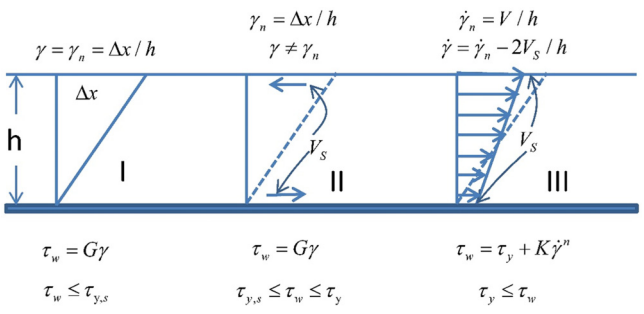

FIG. 4. Schematic illustration of the three flow regimes in simple shear flow.

In agreement with the experiments, the critical apparent shear rate $\dot{\gamma}_{nc}$ at which we have the transition from regime II to regime III is also gap-size dependent,

$$\dot{\gamma}_{nc} = \frac{2}{h}\left(\frac{\tau_y - \tau_{y,s}}{a_1}\right)^{1/m}. \tag{6}$$

Regime III: In this regime, flow is initiated, and the material partially slips. Since the shear rate is $\dot{\gamma} = \dot{\gamma}_n - 2V_S/h$, the apparent flow curve can be generated by means of Eq. (1) subject to slip

$$\tau_w = \tau_y + k(\dot{\gamma}_n - 2V_S/h)^n, \quad \tau_w > \tau_y, \tag{7}$$

where the slip velocity now follows Eq. (3).

Equations (5) and (7) are coupled and can be solved numerically for V_S and τ_w to generate the flow curve for $\tau_w > \tau_y$. It should be emphasized that the transition from regime II to III is not sharp in the parallel-plate flow geometry as the flow field is nonuniform. It is expected that the material starts yielding at the rim first and as the shear rate is increased further, the yielding point propagates inward toward the centerline. The calculations to fit the experimental flow curve should take this into account, i.e., consider the yield point and calculate the contributions to the torque from both the unyielded (inner part of the plates) and the yielded regions (outer part of the plates). It remains to be seen how a simple slip velocity model [Eqs. (2) and (3)] coupled with

the H–B model (rheological behavior of the material) can capture the complex rheological behavior depicted in Fig. 1.

First, the azimuthal velocity in the parallel-plate geometry is given by

$$u(r,z)=\begin{cases}\dot{\gamma}_n h/2, & 0\le r\le r_0,\\ V_s(r)(1-2z/h)+\dot{\gamma}_n z, & r_0\le r\le R,\end{cases} \tag{8}$$

where r_0 is the yield radius (the radius defining the transition from regime II to III in the parallel-plate geometry). This is calculated by noting that the slip velocity in the unyielded core is given by

$$V_s(r)=\frac{\dot{\gamma}_n(r)h}{2}=\frac{\dot{\gamma}_n(R)hr}{2R}. \tag{9}$$

By demanding that the slip velocity at the yield radius, r_0, satisfies Eq. (3), the following expression is obtained for r_0/R:

$$\frac{r_0}{R}=\frac{2}{h\dot{\gamma}_n(R)}\left(\frac{\tau_y-\bar{\tau}_{y,s}}{a_2}\right)^{1/m}. \tag{10}$$

Hence, the yield radius, r_0, is inversely proportional to both the nominal rim shear rate $\dot{\gamma}_n(R)$ and the gap size h. In the yielded core ($r_0\le r\le R$), the slip velocity $V_s(r)$ is calculated by solving the following nonlinear equation [combination of Eqs. (1) and (3)]:

$$\tau_y+k\left[\dot{\gamma}_n(r)-2\frac{V_s(r)}{h}\right]^n=\bar{\tau}_{y,s}+a_2V_s^m(r),\quad r_0\le r\le R. \tag{11}$$

Once the slip velocity is computed, one can easily construct the two-dimensional velocity distribution by means of Eq. (8).

IV. MODELING OF THE EXPERIMENTAL RESULTS

A. Slip calculations

Using the experimental data depicted in Fig. 1, slip was calculated using the Mooney analysis (gap dependence of the flow curve). The slip velocity as a function of shear stress is plotted in Fig. 5 along with fits of the slip model as depicted by Eqs. (2) and (3). There is a jump in the slip velocity at shear stresses around the yield stress. The parameters of the slip model are listed in Table II. A relevant discussion arises with respect to the values of a_1 and a_2 in regimes II and III, respectively. As discussed above, in regime II, slip is solidlike and occurs once the interface fails at the critical "slip" yield stress of $\tau_{y,s}$. Failing of the interface here refers to a rearrangement of particles towards the shear direction at the interface layer. The interface fails since it is weaker in comparison to bulk's yield stress as stress dwindles from a maximum at the moving plate to a minimum at the fixed bottom plate; therefore, the assumption of failing interface before any layer within the bulk is reasonable.

The strength of the interface is related to the modulus of the suspension G_o, which can maintain a fixed deformation when a certain shear stress is applied at the wall, τ_w, $\gamma=\tau_w/G_o$. In this flow regime, the particles specifically at the interface form an immobile layer. However, once the suspension yields and flows, particle migration starts contributing to the increase of slippage demonstrated experimentally by the gap dependence of the flow curves. The mechanism of the slip here is mixed due to the solidlike behavior in regime II plus slip due to additional stress due to flow (velocity gradient). Therefore, it is expected that the slip coefficient should be different in the two flow regimes. The size of the jump in slip velocity is higher in the less concentrated suspensions reflecting the fact that the depletion layer forms easily in less concentrated systems (particle movement is easier). The actual jump in the slip velocity can be calculated by $(a_1/a_2)^{1/m}$, which results in increases of the slip velocity of 129.1, 188, and 77.2 mm/s for kaolinite 18.7, 25, and 31 wt. % respectively.

B. The flow curves

In this section, the predictions of the flow curves are presented by using the slip velocity models [Eqs. (2) and (3)] with the parameters listed in Table I. The parameters of the H–B model [Eq. (1)] are calculated as part of the fitting procedure. While the true yield stress of the material can be uniquely calculated through the fitting procedure, the values of k and n of the H–B model are not fully optimized, and this is mainly due to the limited rheological data. For example, the flow curves used to perform the calculation, include limited data at high shear rates, where the power law according to H–B can be uniquely defined ($\tau\propto\dot{\gamma}^n$ for $\tau\gg\tau_y$). If such data were established, the H–B model parameters could have been uniquely defined. Nevertheless, the procedure used here can also result uniquely the true yield stress of the material. The following steps were used. We initially considered the experimentally determined flow curve using sandpaper as the no-slip flow curve. The Mooney technique using the gap dependence of the flow was used to calculate the slip velocities for each gap; then, results were averaged to represent the trend in slip velocity. Next, the flow curves corresponding to the various gaps were estimated by considering the average calculated slip velocity. The calculated flow curves were corrected for the effects of slip to obtain the no-slip flow curve and were then fitted to the H–B model. This procedure was repeated until convergence, i.e., until obtaining consistent rheological and slip parameters.

Figure 6 depicts the shear stress at the rim as a function of the shear rate for the three kaolinite suspensions. The calculated H–B (converged) parameters are listed in Table II. The main observations from the calculations are as follows: (i) the branch of the flow curve in regime II is initially flat with the shear stress being equal to the slip yield stress $\tau_{y,s}$ and then starts increasing to reach the yield stress value τ_y while the gap dependence is evident from both the experimental data and calculations. The slip yield stress $\tau_{y,s}$ is obtained experimentally, while the true yield stress of the material results from the calculations, although the average values from the plateau values of Fig. 3 are very close and

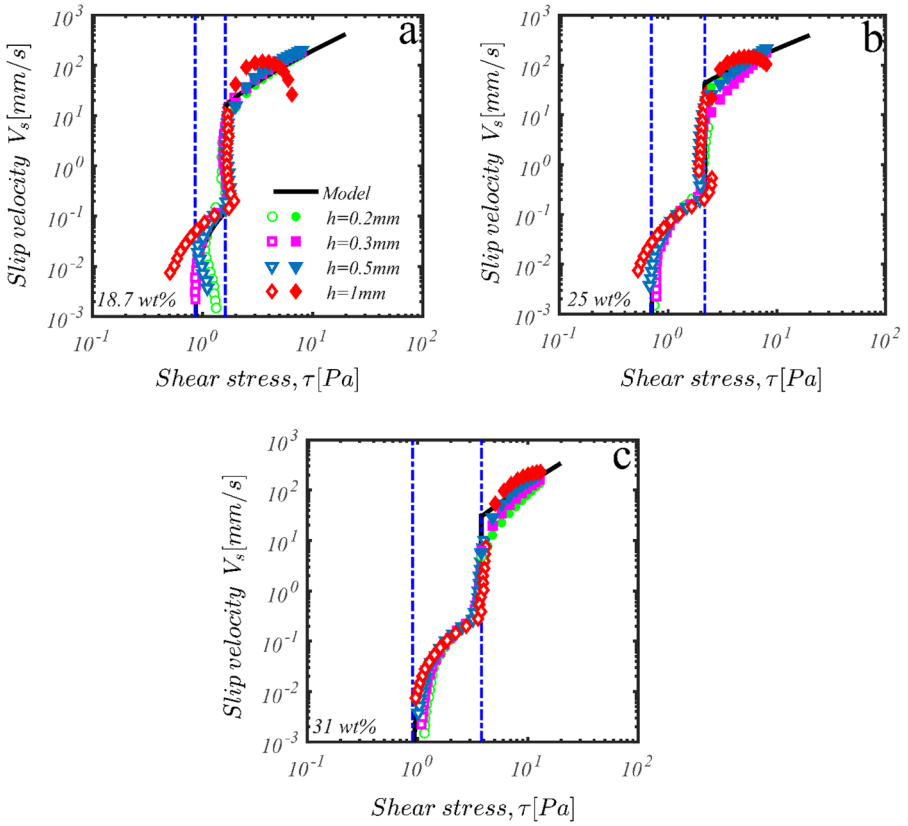

FIG. 5. (a)–(c) Slip velocity versus shear stress using flow curve of kaolinite with a concentration of 18.7–31 wt. % from parallel-plate geometry (50 mm in diameter, and gap size of 0.7 mm) corrected using rough plates with grit 400 at various gap sizes of 0.2–1 mm.

consistent, for various gaps in the parallel-plate geometry and from the cone-and-plate as well as the concentric cylinder geometry. (ii) The flow curve and the gap dependence of the flow curve in regime III are also calculated and agree well with the experimental data.

The above results agree with previous slip studies (experimental and theoretical) in the literature. For example, Péméja and co-workers [39] have reported a systematic experimental investigation of wall slip in a microfluid chip. The authors computed wall shear stress through inference through pressure drop, based on the transversal profile of velocity profile; they selectively identified two slip regimes. Similarly, Seth and co-workers [40], through particle tracking velocimetry, identified two slip regimes separated by an abrupt transition similar to changes seen in Fig. 6 between regimes II and III. They found that for $\tau \geq \tau_y$, the slip velocity would scale linearly with stress and is insensitive to surface properties; however, for $\tau < \tau_y$, the slip velocity was found to be sensitive to the nature of the surfaces.

The proposed model can provide insight into the other interesting parameters that cannot be accessed experimentally. Figures 7 and 8 show the theoretical flow curves, the rim slip velocities, and the yield radii for the parallel-plate flow of the 18.7% and 31% kaolinite suspensions, respectively, obtained for three different gap sizes, i.e., $h = 0.2$, 0.5, and 1 mm, using the calculated rheological and slip parameters listed in Table II. Since the material is unyielded in regime II, the scaled yield radius, r_0/R is unity.

Finally, Fig. 9 illustrates the variation of the slip velocity for four different shear rates, i.e., $\dot{\gamma}_n(R) = 0.2$, 0.5, 1, and 2 in the case of the 18.7% kaolinite suspension. The critical value for the transition from regime II to regime III is $\dot{\gamma}_{nc} = 0.229\ s^{-1}$. Hence, the first value of the shear rate ($0.2\ s^{-1}$) corresponds to regime II, while the other three are in regime III. For

TABLE II. Coefficients of Eqs. (2) and (3) fitted to the data depicted in Fig. 5.

Kaolinite concentration (wt. %)	Regime II		Regime III				Herschel–Bulkley coefficients	
	a_1 (Pa m^{-n} s^n)	m (–)	a_2 (Pa m^{-n} s^n)	m (–)	$\tau_{y,s}$ (Pa)	τ_y (Pa)	k (Pa s^n)	n (–)
18.7	4 993	0.97	44.8	0.97	0.86	1.61	0.004 07	1.01
25	24 379	1.16	56.2	1.16	0.7	2.17	0.003 08	1.09
31	1 241	0.77	43.7	0.77	0.9	3.80	0.095 95	0.70

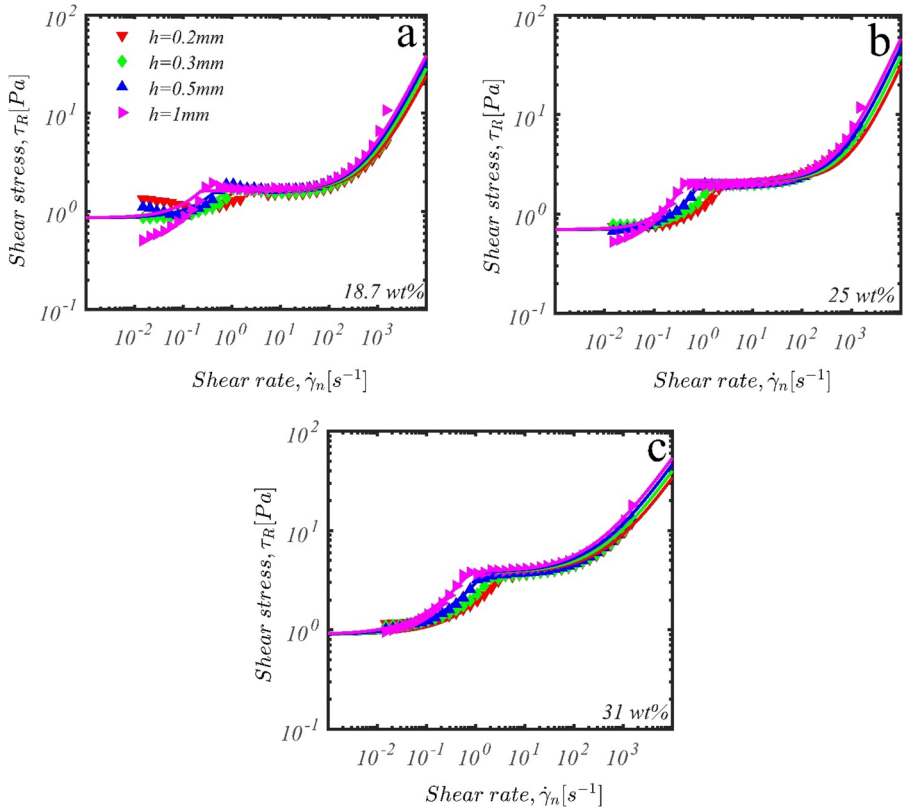

FIG. 6. Comparison of the predicted flow curves with the experimental data for the kaolinite suspensions. (a) Kaolinite 18.7 wt. % and (b) kaolinite 31 wt. %. Continuous lines represent the model predictions at various gaps.

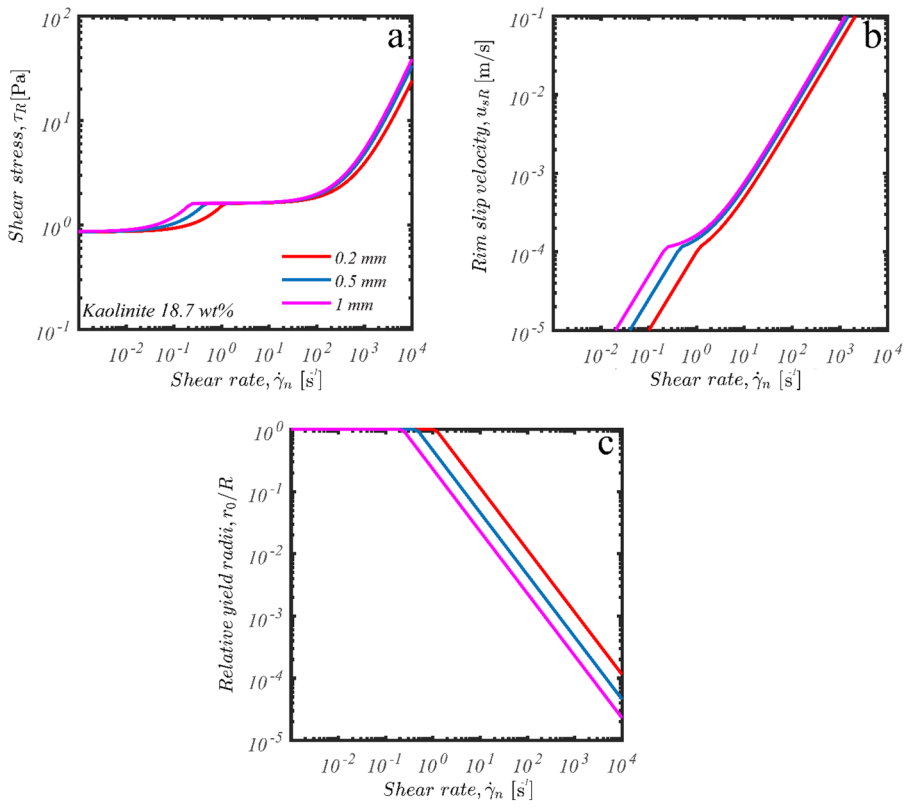

FIG. 7. Predictions for a parallel-plate flow of the 18.7% kaolinite suspension with $h = 0.2$, 0.5, and 1 mm calculated using the parameters given in Table II: (a) flow curves; (b) rim slip velocities; and (c) relative yield radii, r/r_0.

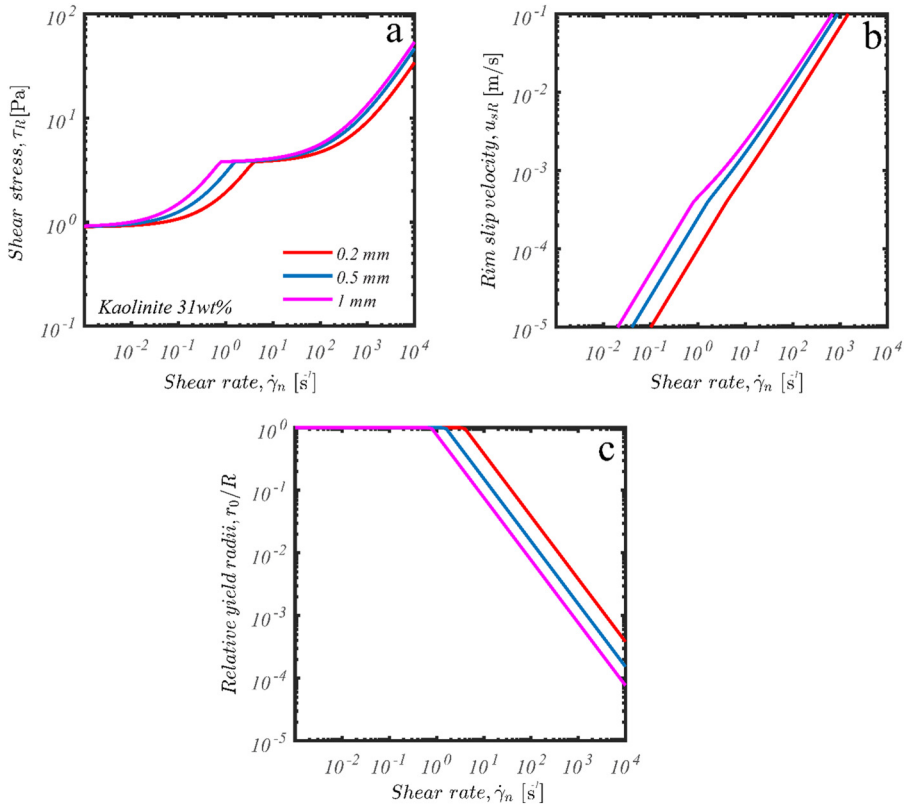

FIG. 8. Predictions for a parallel-plate flow of the 31% kaolinite suspension with $h = 0.2$, 0.5, and 1 mm calculated using the parameters given in Table II: (a) apparent flow curves; (b) rim slip velocities; and (c) relative yield radii $r_{0/R}$.

convenience, the dimensionless angular slip velocity,

$$\omega_s^*(r) = \frac{V_s(r)}{r(h\dot{\gamma}_n/R)} \tag{12}$$

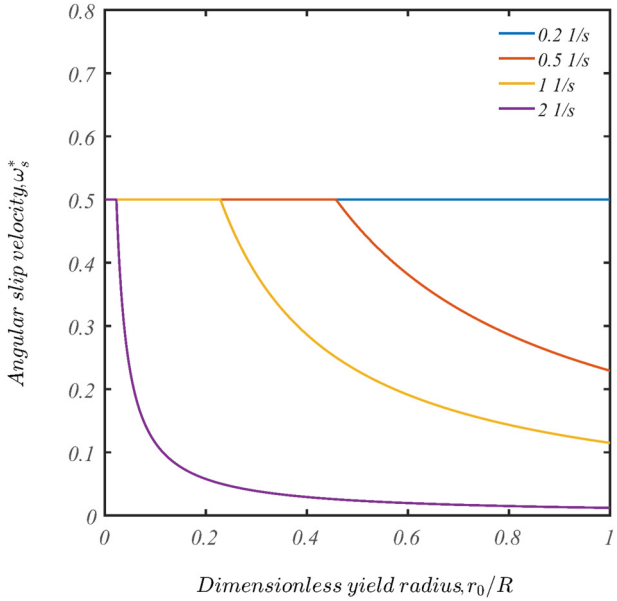

FIG. 9. The dimensionless angular slip velocity $\omega_s^* = V_s(r)/(\dot{\gamma}_n hr/R)$ for various values of the apparent shear rate $\dot{\gamma}_n$ obtained using the rheological and slip parameters corresponding to the 18.7% kaolinite suspension. The critical value for the transition from regime II to regime III is $\dot{\gamma}_{nc} = 0.229\ \text{s}^{-1}$. $\omega_s^* = 1/2$ in the unyielded core. The critical dimensionless yield radii for the three shear rates that are above $\dot{\gamma}_{nc}$ are 0.458, 0.229, and 0.0229.

is plotted, which takes the value of 1/2 in the unyielded core ($0 \le r \le r_0$). The yield radius is calculated by means of Eq. (10). As expected, the yield radius is reduced as $\dot{\gamma}_n(R)$ is increased. The dimensionless angular slip velocity in the yielded region is a decreasing function of the radial distance.

V. CONCLUSIONS

In this study, we have carried out experiments to characterize slip in colloidal suspensions of kaolinite particles and proposed a general slip model that can be applied to many other colloidal systems that possess similar generic features. The rheological measurements were carried out in parallel-plate geometry with smooth and rough plates as well as cone-and-plate and concentric cylinder geometries. The rough surface penetrated the slip layer and created a nonslip region whereas the smooth plate showed a significantly higher slip at higher concentrations of particles. Two separate slip regimes were identified: (i) at shear stresses higher than a critical value referred to as a "slip" yield stress, the material slips in a solidlike fashion (plug flow) that also characterizes the strength (modulus) of the layer at the interface; and (ii) at wall shear stresses above the true yield stress of the material, a depletion layer is formed due to the particle migration causing flow and slip.

The two regimes of slip were modeled by a phenomenological slip velocity model (novelty of this work) that captured the experimental slip data well in all flow regimes. It has been demonstrated that the proposed slip equation along with the H–B constitutive equation describes well the

experimental flow curves of colloidal suspensions for different gaps between the parallel plates. Last but not the least, the proposed methodology seems to yield uniquely the true yield stress and the other rheological parameters. The model was used to study the transition from regime II to regime III, when the suspension yields and flows at the rim of the geometry ($r = R$) and as the shear rate increases, a yielding radius, r_0, is defined. For $r \leq r_0$, the suspension slips in solidlike fashion, whereas for $r > r_0$ the material yields and slips. As the shear rate is increased, the yielding radius propagates toward the centerline and eventually vanishes when the suspension has been fully yielded.

ACKNOWLEDGMENTS

This work was supported by the Natural Sciences and Engineering Research Council (NSERC) of Canada as well as the Institute for Oil Sands Innovation at the University of Alberta (IOSI).

REFERENCES

[1] Buscall, R., "Letter to the editor: Wall slip in dispersion rheometry," J. Rheol. **54**, 1177–1183 (2010).

[2] Yaras, P., D. Kalyon, and U. Yilmazer, "Flow instabilities in capillary flow of concentrated suspensions," Rheol. Acta **33**, 48–59 (1994).

[3] Cloitre, M., and R. T. Bonnecaze, "A review on wall slip in high solid dispersions," Rheol. Acta **56**, 283–305 (2017).

[4] Jung, G., and S. M. Fielding, "Wall slip and bulk yielding in soft particle suspensions," J. Rheol. **65**, 199–212 (2021).

[5] Derzsi, L., D. Filippi, G. Mistura, M. Pierno, M. Lulli, M. Sbragaglia, M. Bernaschi, and P. Garstecki, "Fluidization and wall slip of soft glassy materials by controlled surface roughness," Phys. Rev. E **95**, 052602 (2017).

[6] Leighton, D., and A. Acrivos, "The shear-induced migration of particles in concentrated suspensions," J. Fluid Mech. **181**, 415–439 (1987).

[7] Wilms, P., J. Wieringa, T. Blijdenstein, K. van Malssen, and R. Kohlus, "Quantification of shear viscosity and wall slip velocity of highly concentrated suspensions with non-Newtonian matrices in pressure driven flows," Rheol. Acta **60**, 1–15 (2021).

[8] Divoux, T., C. Barentin, and S. Manneville, "From stress-induced fluidization processes to Herschel-Bulkley behaviour in simple yield stress fluids," Soft Matter **7**, 8409–8418 (2011).

[9] Divoux, T., C. Barentin, and S. Manneville, "Stress overshoot in a simple yield stress fluid: An extensive study combining rheology and velocimetry," Soft Matter **7**, 9335–9349 (2011).

[10] Divoux, T., D. Tamarii, C. Barentin, and S. Manneville, "Transient shear banding in a simple yield stress fluid," Phys. Rev. Lett. **104**, 208301 (2010).

[11] Evans, D. F., and H. Wennerström, "The colloidal domain: where physics, chemistry, biology, and technology meet" (Wiley, NY 1999).

[12] Ballesta, P., R. Besseling, L. Isa, G. Petekidis, and W. Poon, "Slip and flow of hard-sphere colloidal glasses," Phys. Rev. Lett. **101**, 258301 (2008).

[13] Ballesta, P., N. Koumakis, R. Besseling, W. C. Poon, and G. Petekidis, "Slip of gels in colloid–polymer mixtures under shear," Soft Matter **9**, 3237–3245 (2013).

[14] Ballesta, P., G. Petekidis, L. Isa, W. Poon, and R. Besseling, "Wall slip and flow of concentrated hard-sphere colloidal suspensions," J. Rheol. **56**, 1005–1037 (2012).

[15] Israelachvili, J. N., *Intermolecular and Surface Forces* (Academic, London, 2011).

[16] Jiang, T., A. Young, and A. Metzner, "The rheological characterization of HPG gels: Measurement of slip velocities in capillary tubes," Rheol. Acta **25**, 397–404 (1986).

[17] Walls, H., S. B. Caines, A. M. Sanchez, and S. A. Khan, "Yield stress and wall slip phenomena in colloidal silica gels," J. Rheol. **47**, 847–868 (2003).

[18] Meeker, S. P., R. T. Bonnecaze, and M. Cloitre, "Slip and flow in pastes of soft particles: Direct observation and rheology," J. Rheol. **48**, 1295–1320 (2004).

[19] Seth, J. R., M. Cloitre, and R. T. Bonnecaze, "Influence of short-range forces on wall-slip in microgel pastes," J. Rheol. **52**, 1241–1268 (2008).

[20] Ozkan, S., T. Gillece, L. Senak, and D. Moore, "Characterization of yield stress and slip behaviour of skin/hair care gels using steady flow and LAOS measurements and their correlation with sensorial attributes," Int. J. Cosmet. Sci. **34**, 193–201 (2012).

[21] Aktas, S., D. M. Kalyon, B. M. Marín-Santibáñez, and J. Pérez-González, "Shear viscosity and wall slip behavior of a viscoplastic hydrogel," J. Rheol. **58**, 513–535 (2014).

[22] Mooney, M., "Explicit formulas for slip and fluidity," J. Rheol. **2**, 210–222 (1931).

[23] Hatzikiriakos, S. G., and J. M. Dealy, "Wall slip of molten high density polyethylenes. II. Capillary rheometer studies," J. Rheol. **36**, 703–741 (1992).

[24] Yoshimura, A., and R. K. Prud'homme, "Wall slip corrections for Couette and parallel disk viscometers," J. Rheol. **32**, 53–67 (1988).

[25] Hatzikiriakos, S. G., "Slip mechanisms in complex fluid flows," Soft Matter **11**, 7851–7856 (2015).

[26] Hatzikiriakos, S. G., "Wall slip of molten polymers," Prog. Polym. Sci. **37**, 624–643 (2012).

[27] Aral, B. K., and D. M. Kalyon, "Effects of temperature and surface roughness on time-dependent development of wall slip in steady torsional flow of concentrated suspensions," J. Rheol. **38**, 957–972 (1994).

[28] Abbasi Moud, A., J. Poisson, Z. M. Hudson, and S. G. Hatzikiriakos, "Yield stress and wall slip of kaolinite networks," Phys. Fluids **33**, 053105 (2021).

[29] Buscall, R., J. I. McGowan, and A. J. Morton-Jones, "The rheology of concentrated dispersions of weakly attracting colloidal particles with and without wall slip," J. Rheol. **37**, 621–641 (1993).

[30] Bonn, D., H. Kellay, H. Tanaka, G. Wegdam, and J. Meunier, "Laponite: What is the difference between a gel and a glass?," Langmuir **15**, 7534–7536 (1999).

[31] Ovarlez, G., F. Bertrand, and S. Rodts, "Local determination of the constitutive law of a dense suspension of noncolloidal particles through magnetic resonance imaging," J. Rheol. **50**, 259–292 (2006).

[32] Graham, A., S. Altobelli, E. Fukushima, L. Mondy, and T. Stephens, "Note: NMR imaging of shear-induced diffusion and structure in concentrated suspensions undergoing Couette flow," J. Rheol. **35**, 191–201 (1991).

[33] Phillips, R. J., R. C. Armstrong, R. A. Brown, A. L. Graham, and J. R. Abbott, "A constitutive equation for concentrated suspensions that accounts for shear-induced particle migration," Phys. Fluids A **4**, 30–40 (1992).

[34] Corbett, A. M., R. J. Phillips, R. J. Kauten, and K. L. McCarthy, "Magnetic resonance imaging of concentration and velocity profiles of pure fluids and solid suspensions in rotating geometries," J. Rheol. **39**, 907–924 (1995).

[35] Barabé, B., S. Abakumov, D. Gunes, and M. Lettinga, "Sedimentation of large particles in a suspension of colloidal rods," Phys. Fluids **32**, 053105 (2020).

[36] Danesh, M., D. Mauran, S. Hojabr, R. Berry, M. Pawlik, and S. G. Hatzikiriakos, "Yielding of cellulose nanocrystal suspensions in the presence of electrolytes," Phys. Fluids **32**, 93103 (2020).

[37] Coussot, P., Q. D. Nguyen, H. Huynh, and D. Bonn, "Viscosity bifurcation in thixotropic, yielding fluids," J. Rheol. **46**, 573–589 (2002).

[38] Bonn, D., M. M. Denn, L. Berthier, T. Divoux, and S. Manneville, "Yield stress materials in soft condensed matter," Rev. Mod. Phys. **89**, 035005 (2017).

[39] Péméja, J., B. Géraud, C. Barentin, and M. Le Merrer, "Wall slip regimes in jammed suspensions of soft microgels," Phys. Rev. Fluids **4**, 033301 (2019).

[40] Seth, J. R., C. Locatelli-Champagne, F. Monti, R. T. Bonnecaze, and M. Cloitre, "How do soft particle glasses yield and flow near solid surfaces?," Soft Matter **8**, 140–148 (2012).